Chinese Physics B

中国物理学会
Chinese Physical Society

PAPER

Direct observation of the distribution of impurity in phosphorous/boron co-doped Si nanocrystals

To cite this article: Dongke Li *et al* 2023 *Chinese Phys. B* **32** 126102

View the article online for updates and enhancements.

You may also like

- Size and density measurement of core–shell Si nanoparticles by analytical ultracentrifugation
Kanokwan Nontapot, Vinayak Rastogi, Jeffrey A Fagan et al.

- (Invited) Silicon-Based Nano-Composites Made from All-Inorganic Colloidal Silicon Nanocrystals
Minoru Fujii

- Structural and photoluminescence properties of silicon nanowires extracted by means of a centrifugation process from plasma torch synthesized silicon nanopowder
Vincent Le Borgne, Marta Agati, Simona Boninelli et al.

This content was downloaded from IP address 117.28.251.156 on 11/04/2024 at 13:14

Direct observation of the distribution of impurity in phosphorous/boron co-doped Si nanocrystals

Dongke Li(李东珂)[1,2,†], Junnan Han(韩俊楠)[1,†], Teng Sun(孙腾)[1], Jiaming Chen(陈佳明)[1], Etienne Talbot[3], Rémi Demoulin[3], Wanghua Chen(陈王华)[4,‡], Xiaodong Pi(皮孝东)[2], Jun Xu(徐骏)[1,§], and Kunji Chen(陈坤基)[1]

[1] *School of Electronic Science and Engineering, National Laboratory of Solid State Microstructures, Collaborative Innovation Center of Advanced Microstructures, Jiangsu Provincial Key Laboratory of Advanced Photonic and Electronic Materials, Nanjing University, Nanjing* 210000, *China*

[2] *ZJU-Hangzhou Global Scientific and Technological Innovation Center, School of Materials Science and Engineering, Zhejiang University, Hangzhou* 311200, *China*

[3] *Univ Rouen Normandie, INSA Rouen Normandie, CNRS, GPM UMR* 6634, *F-76000 Rouen, France*

[4] *School of Physical Science and Technology, Ningbo University, Ningbo* 315211, *China*

(Received 1 March 2023; revised manuscript received 4 May 2023; accepted manuscript online 23 May 2023)

Doping in Si nanocrystals is an interesting topic and directly studying the distribution of dopants in phosphorous/boron co-doping is an important issue facing the scientific community. In this study, atom probe tomography is performed to study the structures and distribution of impurity in phosphorous/boron co-doped Si nanocrystals/SiO_2 multilayers. Compared with phosphorous singly doped Si nanocrystals, it is interesting to find that the concentration of phosphorous in co-doped samples can be significantly improved. Theoretical simulation suggests that phosphorous–boron pairs are formed in co-doped Si nanocrystals with the lowest formation energy, which also reduces the formation energy of phosphorous in Si nanocrystals. The results indicate that co-doping can promote the entry of phosphorous impurities into the near-surface and inner sites of Si nanocrystals, which provides an interesting way to regulate the electronic and optical properties of Si nanocrystals such as the observed enhancement of conductivity and sub-band light emission.

Keywords: Si nanocrystals, phosphorous and boron, co-doping, impurity distribution

PACS: 61.72.uf, 61.82.Rx, 61.72.U–, 61.72.sh **DOI:** 10.1088/1674-1056/acd7cf

1. Introduction

Due to the potential applications in light emission devices, bio-imaging, neuromorphic computing, etc, Si nanocrystals (NCs) have attracted intensive attention for many years.[1–5] Although much research progress has been achieved, there are still many issues to be addressed, one of which is the doping behaviors in nano-scale Si materials. In the past few years, both theoretical and experimental studies have revealed that the doping effects in Si NCs are quite complicated and different from their bulk counterpart.[6–11] It seems that the introduced impurities tend to locate at the interfacial region rather than the substitutional sites in the core of Si NCs.[12–15] Moreover, due to the novel doping behaviors, one can find some new and interesting phenomena, such as the sub-band light emission in phosphorous (P) doped and P/boron (B) co-doped Si NCs,[16] and localized surface plasmon resonance in B and P hyper-doped Si NCs.[17]

In our previous studies, we focused on the doping effects in Si NCs/SiO_2 multilayers because both the dot size and doping levels can be easily modulated by controlling the preparation parameters.[18,19] More importantly, the whole fabrication process is compatible with CMOS technology. We systematically studied the distribution of impurity in P or B singly doped Si NC samples and the doping-induced novelty in electronic and optical properties.[20–23] We also fabricated P/B co-doped Si NCs/SiO_2 multilayers, and it is interesting to find improved conductivity and enhanced sub-band light emission via suitable co-doping.[16,24] However, direct observation of the distribution of impurities is still lacking and the corresponding mechanism is still unclear.

In this work, we use atom probe tomography (APT) to directly study the structures and the distribution of impurity in P/B co-doped Si NCs/SiO_2 multilayers and compare it with that of a P-singly doped sample. It is found that co-doping can promote the entry of more P impurities into the near-surface and inner sites of Si NCs. Theoretical simulation suggests that the P–B pairs are formed in co-doped Si NCs since they have the lowest formation energy, which also reduces the formation energy of P in Si NCs. The promotion of P in Si NCs due to B co-doping causes the observed enhancement of conductivity and sub-band light emission.

2. Experiment

The P/B co-doped Si/SiO_2 multilayers composed of alternately stacked amorphous Si (a-Si) and SiO_2 sublayers were fabricated by a radio-frequency enhanced plasma-enhanced

[†] These authors contributed equally to this work.
[‡] Corresponding author. E-mail: chenwanghua@nbu.edu.cn
[§] Corresponding author. E-mail: junxu@nju.edu.cn
© 2023 Chinese Physical Society and IOP Publishing Ltd http://iopscience.iop.org/cpb http://cpb.iphy.ac.cn

chemical vapor deposition (PECVD) system. In brief, the mixture gases of SiH_4 (5 sccm), PH_3 (1%, H_2 dilution, 10 sccm), and B_2H_6 (1%, H_2 dilution, 2 sccm) were simultaneously ionized to deposit a P and B co-doped a-Si sublayer on Si wafers or quartz substrates. The gas pressure of the reaction chamber was kept near 20 Pa. The molar atomic ratios of P and B to Si in the mixture gases are 2.0% and 0.8%, respectively, which are also defined as the nominal doping ratios of samples. Meanwhile, the 2.0% P singly-doped sample (PH_3: 10 sccm, B_2H_6: 0 sccm) was deposited for comparison. The SiO_2 sublayer was prepared through *in situ* oxidation of an a-Si sublayer in an oxygen plasma atmosphere. The doped a-Si deposition (90 s) and oxidation processes (90 s) were alternately repeated to obtain the periodically a-Si/SiO_2 multilayered films. Then, the deposited films were annealed under nitrogen gas ambient, and the dehydrogenation temperature was at 450 °C (1 h) and crystallized at 1000 °C (1 h), respectively. Microstructures of Si NC multilayers were characterized by Raman spectroscopy (Horiba HR 800) and cross-sectional TEM (Tecnai G2 F20). Element mapping and distribution were characterized by a UV femtosecond laser-assisted APT system (CAMECA LAWATAP). The computational models and methods are shown in the supplementary material.

3. Results and discussion

Figure 1(a) shows the Raman spectra of as-deposited and annealed P/B co-doped samples. For the as-deposited film, the Raman spectrum exhibits a broad scattering packet near 470 cm^{-1}, which is electrically activated by the transverse optical mode of a-Si.[25] After annealing, the Raman signal of the a-Si becomes weak, while a strong Raman peak appears near 519 cm^{-1}. This is related to the transverse optical mode of the crystallized Si phase and indicates the co-doped sample has been crystallized.[26] Figure 1(b) shows the cross-sectional microstructure of P/B co-doped Si NCs/SiO_2 multilayers investigated by TEM. After high-temperature annealing, the periodically stacked multilayers containing Si and SiO_2 sublayers are kept and the interfaces between the sublayers are smooth and abrupt. The mean thicknesses of SiO_2 and Si sublayers are about 8.0 nm and 4.0 nm, respectively. It is confirmed that Si NCs are uniformly located in the Si sublayers. In at least one direction, the sizes of these Si NCs remain consistent with the thickness of the Si sublayers, which indicates the crystallization size of Si NCs can be well controlled by the multilayered heterostructures.

Femtosecond laser-assisted APT measurements are performed to provide detailed element distribution in the P/B co-doped Si NC samples. Figure 1(c) shows the reconstructed 3D mapping of Si atoms from the APT results. It is clearly observed that the scarce and rich Si regions are alternately stacked, which is consistent with the predesigned multilayered structure. The scarce Si regions with a mean thickness of about 4.0 nm correspond to the SiO_2 sublayers. Meanwhile, the regions richly filled with Si atoms have an average thickness of about 8.0 nm, which corresponds to the Si sublayers. Further, profiles of the concentration of the distribution of Si and O in P/B co-doped multilayers are shown in Fig. 1(d). Periodic variations of Si and O concentrations dependent on the spatial distance can be visually identified, which is also evidence of the multilayered structure of Si and SiO_2 sublayers. The intersections of the Si and O concentration curves, in which the values of Si and O concentrations are both 50.0 at.%, can be designated as the interfacial regions between the Si and SiO_2 sublayers. The statistically averaged Si concentration in the Si sublayers is about 95.6 at.%. For the SiO_2 sublayers, the average concentration of Si and O are 36.0 at.% and 63.9 at.%, respectively.

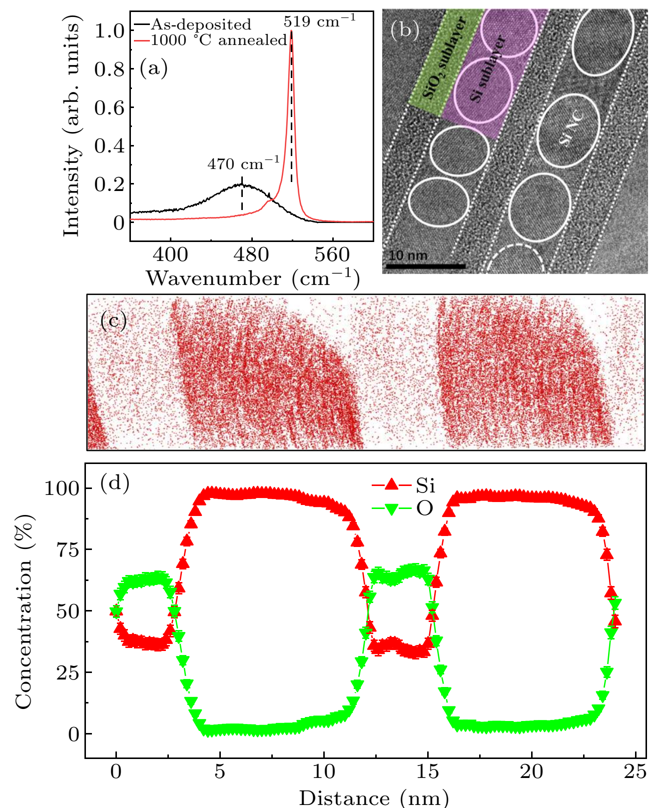

Fig. 1. P/B co-doped Si NCs/SiO_2 multilayers. (a) Cross-sectional TEM image; (b) Raman spectra; (c) APT elemental mapping of Si atoms (7 nm × 7 nm × 24 nm); (d) profiles of the concentration of Si and O compositions. Si and O are plotted in red and green, respectively.

Furthermore, the distributions of P and B impurities in co-doped samples are studied at the atomic scale. Figures 2(a) and 2(b) show the APT mapping of P and B impurities, respectively. The distribution of O atoms is also given to exhibit the structure of the multilayers. It is found that P impurities are mainly located at the interfacial regions between the Si and SiO_2 sublayers, and part of them are also distributed at the inner Si and SiO_2 sublayers. The P impurities in the SiO_2 sublayers are attributed to the fact that the SiO_2 sublayers are

fabricated by *in situ* oxidation of doped a-Si sublayers during the preparation process. Although a high-temperature annealing process has also been performed, some impurities still remain in the SiO_2 sublayer due to the stable chemical structure of SiO_2 and the low thermal mobility of impurities in SiO_2. In a previous study, we found that P impurities are relatively uniformly distributed in the as-deposited P singly-doped a-Si sublayers, in which P impurities are redistributed with the formation of Si NCs under high-temperature annealing.[27] Besides, most of the P impurities are finally located at the interfacial regions of the Si sublayers, i.e., the near-surface of Si NCs, and part of the remaining P impurities in the Si sublayers can be electrically activated in the lattice sites of Si NCs.[27] As shown in Fig. 2(b), B impurities are also mainly distributed at the interfacial regions and the content in the Si sublayers can be negligible, which is quite different from B impurities that can form the boron aggregations in B singly-doped Si NCs.[27] This indicates that B impurities exhibit a different doping mechanism in co-doped and singly-doped Si NCs.

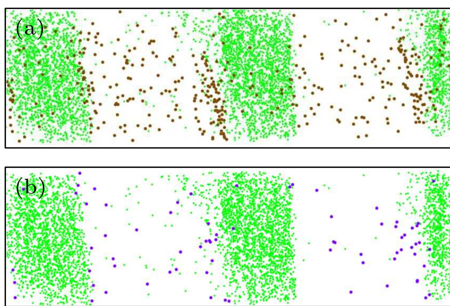

Fig. 2. APT elemental mapping (8 nm × 8 nm × 24 nm) of P/B co-doped sample. (a) O and P atoms; (b) O and B atoms. O, P, and B are plotted in green, olive, and violet, respectively.

Figure 3(a) shows profiles of the concentration of P and B impurities in the P/B co-doped sample, and that of P impurities in the 2% P singly-doped sample is shown in Fig. 3(b) for comparison. P impurities show similar distribution characteristics of preferentially occupying the interface positions in single doping and co-doping. This can be explained by the self-purification effect in which NCs tend to push the impurities out to keep the stable crystalline structure and smallest formation energy. It is interesting to find that the average P concentration in the Si sublayers of the co-doped sample can reach 0.74 at.%, which is much higher than that of 0.45% for the P singly-doped sample with the same doping ratio of 2%. The higher concentration of impurity in the Si sublayers will inevitably lead to more impurities being located at the lattice sites of Si NCs and electrically activated. This direct observation result at the atomic scale is in good accordance with previous reports showing P doping efficiency and carrier concentrations in Si NCs can be improved via B co-doping at suitable levels.[24] In addition, the error bars shown in Fig. 3 refer to the statistical incertitude of the time-of-flight mass spectrometry in the APT measurement.

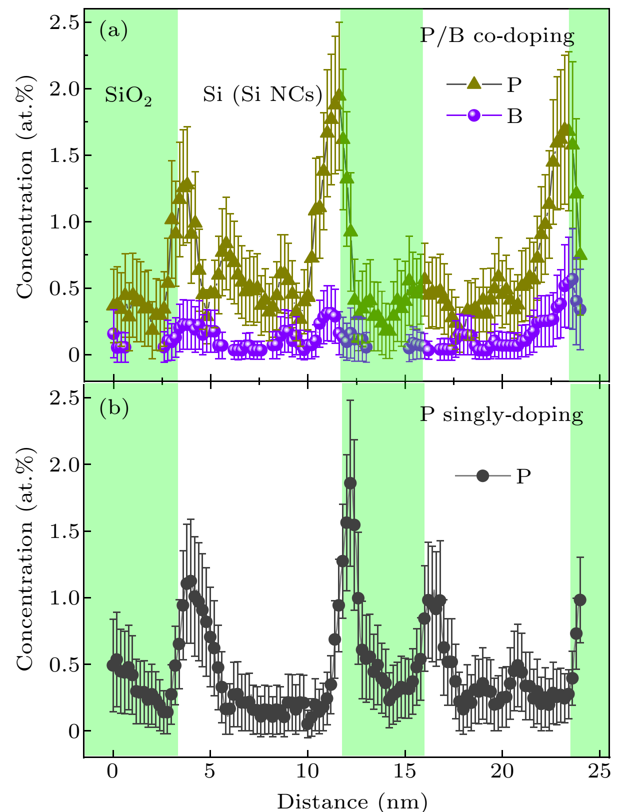

Fig. 3. (a) Profiles of the concentration of P and B impurities in the P/B co-doped sample. (b) Profiles of the concentration of P impurities in the P singly-doped sample for comparison. B and P are plotted in violet and olive (or black), respectively.

In order to further understand the experimental observations of the behaviors of the distribution of impurity in Si NCs, first-principles theoretical calculations have been performed to obtain the formation energy of the impurity in the various sites of Si NCs surrounded by SiO_2 by taking into account the existence of dangling bonds on the surface. Figure 4(a) illustrates the formation energy of P or B impurity in the singly doped sample. Four sites are considered, which are the inner site, subsurface site (Si_s), interfacial site (Si_i) as well as the site in SiO_2, respectively. After passivation of dangling bonds, it is found that P impurities can enter the Si NCs but B atoms tend to stay at the interfacial sites. Figure 4(b) shows the formation energy of B impurities in a co-doped sample when the dangling bonds are passivated by P. The calculated formation energy of P impurities in a co-doped sample when the dangling bonds are passivated by B is shown in Fig. 4(c). It looks like the formation energy is almost the same as that in the singly doped one but the formation energy of P impurities at the inner site, Si_s, and Si_i becomes smaller as shown in Fig. 4(c), which means the P atoms may have more possibility to enter into the Si NCs in the co-doped case.

We also find another interesting result where the P–B pairs in the interfacial sites have the lowest formation energy

as indicated in Figs. 4(b) and 4(c). It is suggested that P/B co-doping can promote the formation of P–B pairs in the interfacial region of Si NCs. Fujii and coworkers studied the distribution of impurities in freestanding co-doped Si NCs.[28] They found that the formation of P–B pairs in samples and the percentage of P–B pairs was increased with annealing temperature due to the reduction of formation energy. The existence of P–B pairs caused the low photoluminescence energy below the bandgap of bulk Si.[8,29] Meanwhile, Guerra *et al.* calculated the preferential position of impurities in co-doped Si NCs by considering the OH termination.[30] They also found that the P–B pair at the interfacial region was the most energetically favored sites, which resulted in a stable permanent electric dipole that radially points inward in Si NCs. In our case, the studied sample is P/B co-doped Si NCs/SiO_2 multilayers, which is similar to the theoretic calculation model by Guerra *et al.*; the Si NCs' surface is covered by oxygen and a strong charge trapping is predicted at the surface oxygen. P–B pairs are easily formed in the interface regions and P is located inside of the Si NCs to get more stable configurations.[30]

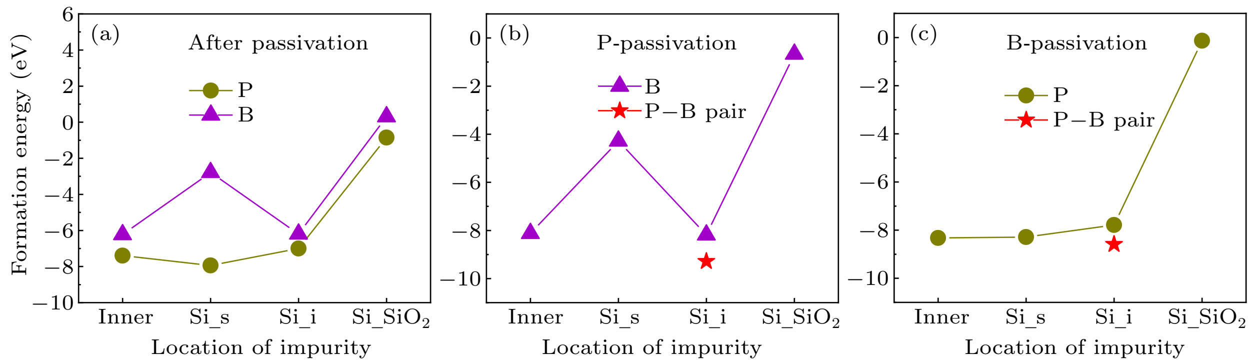

Fig. 4. (a) Formation energy curves of P and B impurities as a function of doping sites after the dangling bond is passivated. (b) Formation energy curves of B impurity varying with co-doping sites after the dangling bonds were passivated by P. (c) Formation energy curves of P impurity vary with co-doping sites after the dangling bonds were passivated by B.

Figure 5 shows the formation energy of P or B impurities in the co-doped sample after considering the existence of P–B pairs. The calculated results imply that both the formation energy of P and B becomes smaller than that in the singly-doped sample. Especially for P impurities, the calculation results are obviously decreased in the inner and subsurface sites compared with the value given in Figs. 4(a) and 4(c). This suggests that P/B co-doping can make more P impurities enter the Si NCs, which is in good agreement with the APT observations as we discussed before. Since the atom radius of Si, P, and B is 0.110 nm, 0.100 nm, and 0.085 nm, respectively,[31] the difference between Si and P is obviously smaller than that between Si and B. Therefore, P impurities can easily be substitutional doping in Si NCs but this is more difficult with B impurities compared to P atoms due to the large structural change and in turn the strong stress in Si NCs, especially small-sized dots. By P/B co-doping, P–B pairs can be formed in the interfacial region, which results in more B impurities remaining at the interfacial sites and relaxing the structures to release the stress. Meanwhile, more P impurities, which have almost the same atom radius as Si, can be incorporated into the inner sites and subsurface sites as revealed by our theoretical and experimental studies. In our previous work, we found that the electron density is increased by P/B co-doping and the sub-band light emission in P-doped Si NCs with ultra-small sizes can be enhanced by suitable B co-doping;[16] the above results can be understood in terms of more P impurities being promoted into the Si NCs due to the B co-doping and it provides an interesting way to control the electronic and optical properties of Si NCs.

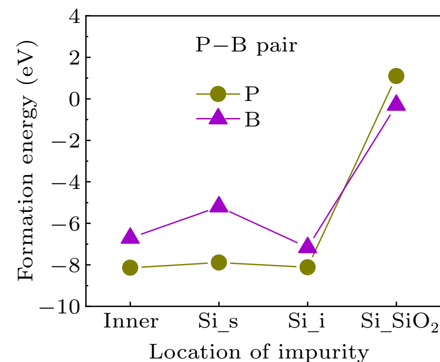

Fig. 5. Formation energy curves of P and B impurities varying with the co-doping site after the dangling bonds were passivated by the P–B pair.

4. Summary

P/B co-doped Si NCs/SiO_2 multilayers are fabricated by a PECVD system and an annealing process. Under the constrained crystallization effect of a multilayered structure, Si NCs are uniformly distributed in Si sublayers, and the size is constrained in at least one direction. APT analyses indicate that P and B impurities are mainly located at the interfacial regions between the Si and SiO_2 sublayers. Compared with the P singly-doped sample, the concentrations of P impurities in the P/B co-doped Si sublayers are significantly improved, which indicates co-doping can promote the entry of more P impurities into the near-surface and inner sites of Si NCs. Theoretical

simulation suggests the formation energies of P and B in co-doped samples become smaller than that in singly-doped samples. Furthermore, the P–B pairs can be formed in co-doped Si NCs with the lowest formation energy, while the formation energy of P impurities is obviously decreased in the inner and subsurface sites, which is in good agreement with the APT observations. The promotion of P in Si NCs due to B co-doping provides an interesting way to control the electronic and optical properties of Si NCs.

Acknowledgments

Project supported by the National Key Research and Development Program of China (Grant No. 2018YFB2200101), the National Natural Science Foundation of China (Grant Nos. 62004078 and 61921005), Natural Science Foundation of Jiangsu Province (Grant No. BK20201073), Natural Science Foundation of Ningbo (Grant No. 2021J068), ANR DONNA (Grant No. ANR-18-CE09-0034), and Leading Innovative and Entrepreneur Team Introduction Program of Hangzhou (Grant No. TD2022012). This work was partially supported by the CNRS Federation IRMA-FR 3095.

References

[1] Hao H, Zhao Y, Song T, Wang X, Li C, Li W and Shen W 2021 *Nanotechnology* **32** 505611
[2] Fujii M, Fujii R, Takada M and Sugimoto H 2020 *Acs Appl. Nano Mater.* **3** 6099
[3] Cao Y Q, Zhu P, Li D K, Zeng X H and Shan D 2020 *Energies* **13** 4845
[4] Tan H, Ni Z Y, Peng W B, Du S C, Liu X K, Zhao S Y, Li W, Ye Z, Xu M S, Xu Y, Pi X D and Yang D R 2018 *Nano Energy* **52** 422
[5] Wang J, Ye D X, Liang G H, Chang J, Kong J L and Chen J Y 2014 *J. Mater. Chem. B* **2** 4338
[6] Ni Z Y, Zhou S, Zhao S Y, Peng W B, Yang D R and Pi X D 2019 *Mater. Sci. Eng. R* **138** 85
[7] Li D, Xu J, Zhang P, Jiang Y and Chen K 2018 *J. Phys. D-Appl. Phys.* **51** 233002
[8] Sugimoto H, Yamamura M, Fujii R and Fujii M 2018 *Nano Lett.* **18** 7282
[9] Marri I, Degoli E and Ossicini S 2017 *Prog. Surf. Sci.* **92** 375
[10] Oliva-Chatelain B L, Ticich T M and Barron A R 2016 *Nanoscale* **8** 1733
[11] Ni Z Y, Pi X D, Cottenier S and Yang D R 2017 *Phys. Rev. B* **95** 075307
[12] Nomoto K, Sugimoto H, Ceguerra A V, Fujii M and Ringer S P 2020 *Nanoscale* **12** 7256
[13] Lu P, Mu W, Xu J, Zhang X, Zhang W, Li W, Xu L and Chen K 2016 *Sci. Rep.* **6** 22888
[14] Li D, Jiang Y, Liu J, Zhang P, Xu J, Li W and Chen K 2017 *Nanotechnology* **28** 475704
[15] Pi X D, Gresback R, Liptak R W, Campbell S A and Kortshagen U 2008 *Appl. Phys. Lett.* **92** 123102
[16] Li D, Chen J, Sun T, Zhang Y, Xu J, Li W and Chen K 2022 *Opt. Express* **30** 12308
[17] Kramer N J, Schramke K S and Kortshagen U R 2015 *Nano Lett.* **15** 5597
[18] Chen J, Li D, Zhang Y, Jiang Y, Xu J and Chen K 2020 *Appl. Surf. Sci.* **529** 146971
[19] Jiang Y, Li D, Xu J, Li W and Chen K 2018 *Appl. Surf. Sci.* **461** 66
[20] Zhang P, Li S, Li D, Ren L, Qin Z, Jiang L and Xu J 2023 *Opt. Laser Technol.* **157** 108706
[21] Chen J, Li D, Sun T, Han J, Wang L, Zhang Y, Xu J and Chen K 2022 *Opt. Mater. Express* **12** 4096
[22] Lu P, Li D, Zhang P, Tan D, Mu W, Xu J, Li W and Chen K 2016 *Opt. Mater. Express* **6** 3233
[23] Qian M, Shan D, Ji Y, Li D, Xu J, Li W and Chen K 2016 *Nanoscale Res. Lett.* **11** 346
[24] Li D, Jiang Y, Zhang P, Shan D, Xu J, Li W and Chen K 2017 *Appl. Phys. Lett.* **110** 233105
[25] Shan D, Ji Y, Li D, Xu J, Qian M, Xu L and Chen K 2017 *Appl. Surf. Sci.* **425** 492
[26] Fukata N 2009 *Adv. Mater.* **21** 2829
[27] Li D, Chen J, Xue Z, Sun T, Han J, Chen W, Talbot E, Demoulin R, Li W, Xu J and Chen K 2023 *Appl. Surf. Sci.* **609** 155260
[28] Nomoto K, Sugimoto H, Breen A, Ceguerra A V, Kanno T, Ringer S P, Wurfl I P, Conibeer G and Fujii M 2016 *J. Phys. Chem. C* **120** 17845
[29] Hori Y, Kano S, Sugimoto H, Imakita K and Fujii M 2016 *Nano Lett.* **16** 2615
[30] Guerra R and Ossicini S 2014 *J. Am. Chem. Soc.* **136** 4404
[31] Slater J C 1964 *J. Chem. Phys.* **41** 3199